WILEY QUANTUM CHEMISTRY International Journal of

FULL PAPER

Uncontracted basis sets for ab initio calculations of muonic atoms and molecules

Mihkel Ugandi[1] [ID] | Ignacio Fdez. Galván[1] | Per-Olof Widmark[2] | Roland Lindh[1]

[1]Department of Chemistry – Ångström, The Theoretical Chemistry Programme, Uppsala University, Uppsala, Sweden

[2]Department of Theoretical Chemistry, Lund University, Lund, Sweden

Correspondence
Prof. Roland Lindh, Department of Chemistry - Ångström, Uppsala University, Box 538, 751 21 Uppsala, Sweden.
Email: roland.lindh@kemi.uu.se

Funding information
Swedish Research Council, Grant/Award Number: Grant 2016-03398

Abstract

In this work, we investigated muonic atoms and molecules from a quantum chemist's viewpoint by incorporating muons in the CASSCF model. With the aim of predicting muonic X-ray energies, primitive muonic basis sets were developed for a selection of elements. The basis sets were then used in CASSCF calculations of various atoms and molecules to calculate muonic excited states. We described the influence of nuclear charge distribution in predicting muonic X-ray energies. Effects of the electronic wave function on the muonic X-ray energies were also examined. We have computationally demonstrated how the muon can act as a probe for the nuclear charge distribution or electronic wave function by considering lower or higher muonic excited states, respectively.

KEYWORDS

CASSCF, muonic basis sets, nuclear charge distribution, quantum chemistry, X-ray spectroscopy

1 | INTRODUCTION

Even though chemists are primarily concerned with ordinary substances consisting of electrons and atomic nuclei, the families of subatomic particles allow for various additional types of exotic matter. For example, the positive muon can replace the proton in a hydrogen atom to yield a light isotope of hydrogen called muonium. The muonium atom can then become a part of molecules and give rise to structural changes.[1] In addition, positive muons can localize in condensed matter at negatively charged sites.[2] The localization of positive muons in matter is of interest to experimentalists working with the muon spin resonance/rotation/relaxation (μSR) technique.[3] Quite recently there have been computational studies on small organic molecules where one of the protons has been substituted with a positive muon. Localization of the muon and the muonic hyperfine coupling constant have been predicted to demonstrate how the positive muon can act as a probe for molecular structure.[4–6]

Negative muons, conversely, can replace electrons in atoms and molecules. Muonic atom formation in particular, has been a well-known phenomenon for several decades.[7] Due to the muon being approximately 200 times heavier than an electron, its orbitals are significantly more compact. This leads to the muon shielding the nucleus from electrons by almost one unit charge.[8] The process of muonic atom formation is accompanied by the emission of X-rays which originate from the cascading of the muon down to lower energy states. These muonic X-ray energies are primarily determined by the nuclear charge but also by the size of the nucleus and to a lesser extent by electronic structure.[8] The free muon's lifetime is 2.2 μs and it is reduced to some extent in muonic atoms by nuclear capture processes.[8–10] Recently, there have been interesting developments in muonic X-ray spectroscopy where nondestructive elemental analysis with several useful properties has been achieved.[11–13] This in turn has awakened the interest of theoreticians, who can use quantum mechanics to predict properties of muonic atoms and molecules.

Reyes and co-workers have developed specialized muonic basis sets and then investigated muonic atoms ranging from hydrogen to argon at Hartree–Fock (HF) and full configuration interaction (FCI) levels of theory. Shielding of the nuclear charge by the muon and its effect on ionization potentials were studied in detail.[14–16] However, works which aim at bridging muonic X-ray spectroscopy and theoretical prediction of muonic X-ray energies have been missing. We attempt to narrow this gap by developing muonic basis sets and using them to calculate muonic X-ray energies for a selection of atoms and molecules.

2 | THEORY

The equations which incorporate muons in the HF and configuration interaction (CI) models can be found in the work by Posada et al.[16] In our study, the CI method is combined with orbital optimization, yielding a complete active space self-consistent field (CASSCF) method which is capable of calculating muonic excited states with ground state electronic configuration.[17] The calculation of molecular integrals over mixed electronic/muonic basis sets was handled as follows. The one-particle integrals $\left(i|\hat{h}|j\right)$ are nonvanishing only if the indices i, j both refer to either electronic or muonic basis functions. This is so since the operator $\hat{h}$ contains either muonic or electronic operators of kinetic energy and Coulombic attraction with the nucleus. Regarding two-particle integrals, because electrons and muons are mutually distinguishable, there can only be electron-muon Coulomb integrals and no electron-muon exchange integrals. Therefore, the two-particle integrals (ij|kl) are nonvanishing only when i, j both refer to electrons or muons and k, l both refer to electrons or muons.

Due to the muon's larger mass compared with an electron, there are few additional issues that need to be taken care of. First, the Born–Oppenheimer approximation becomes less valid for treating muonic atoms and molecules. To compensate for this, we implemented the finite nuclear mass correction (FNMC) developed by Mohallem and coworkers.[18,19] Recently FNMC was successfully applied by Reyes and coworkers to correct for the Born–Oppenheimer approximation in their study of muonic atoms.[15,16] In the FNMC method, the electronic or muonic kinetic energy integrals

$$T_{ijAB} = -\frac{1}{2m}\langle\phi_{iA}|\nabla^2|\phi_{jB}\rangle \tag{1}$$

are modified by addition of the quantity

$$Q_{ijAB} = \begin{cases} \frac{m}{M_A}T_{ijAB} & \text{if } A = B \\ 0 & \text{if } A \neq B \end{cases} \tag{2}$$

where m is the mass of electron or muon, M_A is the mass of nucleus A and T_{ijAB} is the electronic or muonic kinetic energy integral. The small letter indices i and j denote the basis functions and the capital letter indices A and B specify the nuclei at which the basis functions are centered. Then, at the Hartree–Fock level, the Fock matrix is corrected by adding the FNMC matrix $\mathbf{Q}$ to the Born–Oppenheimer Fock matrix $\mathbf{F}$,

$$\mathbf{F}_{FNMC} = \mathbf{F} + \mathbf{Q} \tag{3}$$

Because the kinetic energy matrix elements are modified, the correction also affects correlated methods. Formally, in the CASSCF method, the correction modifies the Hamiltonian matrix which is to be diagonalized.

Second, because of the muon's large mass, its orbitals are significantly closer to the nucleus. Therefore, assuming a point-like structure of the nucleus is expected to become inaccurate for predicting muonic energy levels. For modeling the finite size of the nucleus, there are various options like the uniformly charged sphere, the Fermi two-parameter charge distribution and the Gaussian charge distribution.[20] In our work, we make use of the latter. In this model, the nuclear charge distribution of nucleus A is given by

$$\rho_A(R) = \rho_A^0 \exp\left(-\xi_A R^2\right) \tag{4}$$

$$\rho_A^0 = eZ\left(\frac{\xi_A}{\pi}\right)^{3/2} \tag{5}$$

$$\xi_A = \frac{3}{2\langle R^2\rangle} \tag{6}$$

where the nuclear charge distribution parameter ξ_A is related to the empirical root-mean square radius of the nucleus $\langle R^2\rangle$ (see Ref. [20]). Then, in the Hamiltonian, the Coulombic attraction term with the nucleus is modified as follows

$$\hat{V}_{iA} = -\frac{Z_A}{|\mathbf{r_i} - \mathbf{R_A}|} \rightarrow \hat{V}_{iA} = -\int_{V_A}\frac{\rho_A(\mathbf{R_A})}{|\mathbf{r_i} - \mathbf{R_A}|}dV \tag{7}$$

where the charge density integrated over the coordinates of nucleus A yields the nuclear charge Z_A. One of the advantages of the Gaussian nuclear charge distribution is its ease of implementation since molecular integrals over Gaussian functions are routinely calculated in quantum chemical codes.

3 | METHODS

The computational work consisted of optimizing uncontracted muonic basis sets for a selection of elements and then using these basis sets in calculations of muonic atoms and molecules. To lessen concerns about relativistic effects, we considered only lighter elements of the first three rows with the exception of copper. Incorporating basis sets for Cu was done due to the availability of experimental data on muonic X-rays and our

interest in looking at the nuclear size effects on muonic X-ray energies. To have the flexibility for describing a large range of excited states and atoms with varying nuclear charge distribution, the muonic basis sets were not contracted.

3.1 | Optimization of primitive muonic basis sets

The design of primitive muonic basis sets amounted to choosing a number of Gaussian primitives and optimizing their exponents. For the optimization, we considered a hydrogen-like system with one muon and a point-like nucleus. The Gaussian exponents were optimized separately for different orbital angular momentum shells. This yielded different sets of real spherical harmonic Gaussian basis functions for s, p, and d orbitals, covering up to $n = 7$ lowest-energy states.

To avoid the excessive overhead of optimizing Gaussian exponents individually, various options are available that reduce the number of optimization parameters. Commonly, the set of exponents is expressed through even-tempered or well-tempered series.[21] We aimed for greater flexibility and used the so-called polynomial generator functions to expand the Gaussian exponents ($\alpha_k^{(l)}$) as

$$\ln \alpha_k^{(l)} = a_1^{(l)} + \sum_{i=2}^{m} a_i^{(l)} g_i(k) \quad k = 1, \ldots, N_l \tag{8}$$

where N_l is the number of basis functions for given angular momentum atomic orbitals. The polynomial generator functions are defined as $g_i(k) = k^{i-1}$, and the set $\{a_j\}_{j=1}^{m}$ contains the parameters to be optimized-in our work $m = 4$. For the optimization procedure, we used the Nelder–Mead algorithm available in Python's SciPy library.[22,23] The exponents were optimized by minimizing the state-averaged energy obtained from a FCI calculation. The D_{2h} point group was used to partition orbitals of different symmetry. Then, orbitals of particular symmetry were chosen to generate the excited configurations in a FCI calculation. For s, p, and d functions, the energies were averaged over 7, 6, and 5 states, respectively.

3.2 | Calculations on atoms and molecules

After obtaining the basis sets, we did CASSCF calculations on various atoms and molecules to predict muonic excited states and muonic X-ray energies. We looked at the atomic species C, O, Al$^+$, Cu$^+$, Ar, and Ar^{2+} and molecules H_2O and CH_2O. One muon was added to each, decreasing the total charge by one. In the case of molecules, the muonic basis sets were centered on the most electronegative atom. To account for the shielding of nuclear charge by the muon, we used electronic basis sets which correspond to the element with one less atomic number: C-B.ANO-L-VTZP, O-N.ANO-L-VTZP, Al-Mg.ANO-L-VTZP, and Cu-Ni.ANO-L-VTZP.[24–26] For the atoms in the molecule not hosting the muon, we used the normal ANO-L-VTZP basis set. Muons were described using our developed Gaussian primitive basis sets. In the CASSCF calculation, muonic orbitals were put in the active space and the number of active electrons (ie, muons) was set to one. The electrons were included in the inactive space. Doing so we were able to calculate excited states corresponding to muonic excitations. Finally, muonic X-ray energies were calculated as a difference of energies between states with different principal and angular quantum numbers ($\Delta l = 1$). All the implementations and calculations were done using OpenMolcas quantum chemistry software.[27,28]

4 | RESULTS AND DISCUSSION

Primitive muonic basis sets were designed for the atoms H to Ar and Cu. Compared to electronic orbitals, the orbitals of muons are significantly more compact due to the muon's larger mass. This causes the Gaussian exponents of muonic basis sets to be much larger. For example, when comparing the muonic basis sets of Ar with corresponding cc-pVTZ electronic basis sets, the largest and smallest muonic Gaussian exponents for s orbitals are roughly $2 \cdot 10^4$ times larger. The Gaussian exponents for the muonic basis sets we used in our calculations can be found in the Supporting Information.

4.1 | Nuclear size effects

From previous theoretical and experimental studies it is known that changes in the nuclear size and shape, caused for example by the change in the number of neutrons, significantly influence muonic X-ray energies.[29–32] In the model we used, the nuclear charge distribution is determined by a single empirical parameter, the width of the Gaussian distribution, see Equations (4)-(6). To demonstrate the use of our muonic basis sets, we predicted the energies of various muonic transitions in atoms. We calculated the muonic X-ray energies using a point-like and the Gaussian-shaped model for the nucleus. In the latter case, default values taken from Visscher et al. were used.[20] The results of our calculations are shown in Table 1. The calculations were done on systems only with a closed electronic shell and the charges are not consistent among the species studied. Here, we considered only lower level transitions and hence the electronic screening effect is expected to be unimportant.[33] First, we can see that a point-like description of the nucleus gives more accurate results compared to

TABLE 1 Muonic X-ray energies calculated with a point-like (A) and a Gaussian-shaped (B) nucleus with a default parameter ξ, using our developed muonic basis sets. For comparison we have taken available experimental values from Engfer et al. and the so-called typical values from Kubo et al.[7,33,34] For the experimental values of Cu, we have given ranges which cover different states resulting from addition of spin and orbital angular momentum. For the typical values, we have given the Siegbahn notation for the transition in parentheses as given in the reference and interpreted the numbers correspondingly[35]

Transition	A	B	Experimental values	Typical values
μC^-		($\xi = 6.808 \cdot 10^8$)		
$2p \rightarrow 1s$	75.24	74.84	75.25	75.8 (K_α)
$3p \rightarrow 1s$	89.18	88.78	89.21	89.2 (K_β)
$3p \rightarrow 2s$	13.93	13.88		13.9 (L_α)
$3d \rightarrow 2p$	13.93	13.93		13.9 (L_α)
$4p \rightarrow 2s$	18.81	18.76		18.8 (L_β)
$4d \rightarrow 2p$	18.81	18.81		18.8 (L_β)
μO^-		($\xi = 5.863 \cdot 10^8$)		
$2p \rightarrow 1s$	134.08	132.67	133.52	134 (K_α)
$3p \rightarrow 1s$	158.91	157.50	158.41	158 (K_β)
$3p \rightarrow 2s$	24.83	24.65		24.8 (L_α)
$3d \rightarrow 2p$	24.83	24.83		24.8 (L_α)
$4p \rightarrow 2s$	33.52	33.34		33.5 (L_β)
$4d \rightarrow 2p$	33.52	33.52		33.5 (L_β)
μAl		($\xi = 4.434 \cdot 10^8$)		
$2p \rightarrow 1s$	355.07	343.67	346.9	347 (K_α)
$3p \rightarrow 1s$	420.83	409.43	413.02	422 (K_β)
$3p \rightarrow 2s$	65.75	64.32		65.8 (L_α)
$3d \rightarrow 2p$	65.75	65.75		65.8 (L_α)
$4p \rightarrow 2s$	88.76	87.33		88.8 (L_β)
$4d \rightarrow 2p$	88.76	88.76		88.8 (L_β)
μAr^-		($\xi = 3.572 \cdot 10^8$)		
$2p \rightarrow 1s$	681.66	637.12	643.94	
$3p \rightarrow 1s$	807.89	763.34		
$3p \rightarrow 2s$	126.23	120.58		
$3d \rightarrow 2p$	126.23	126.22		
$4p \rightarrow 2s$	170.41	164.76		
$4d \rightarrow 2p$	170.41	170.39		
μCu		($\xi = 2.767 \cdot 10^8$)		
$2p \rightarrow 1s$	1771.19	1495.77	1506.61 - 1512.78	1513 (K_α)
$3p \rightarrow 1s$	2099.19	1823.51		2126 (K_β)
$3p \rightarrow 2s$	328.00	292.40		307 (L_α)
$3d \rightarrow 2p$	328.00	327.61	330.26 - 334.80	307 (L_α)
$4p \rightarrow 2s$	442.79	407.11		444 (L_β)
$4d \rightarrow 2p$	442.79	442.40		444 (L_β)

experimental values for the lighter C and O atoms. However, for the species Al, Ar and especially Cu, using the Gaussian model for the nucleus yields energies closer to the experiment. Unfortunately, with the default values the energies are still somewhat off.

In comparison with the typical muonic X-ray energies given in Kubo et al., we can identify larger discrepancies.[7,34] At first for the C and O atoms, our calculations compare quite well. However, when looking at the heavier atoms, we can see significant differences arising. For Al and Cu, the K_β transitions are lower both in our calculations and the experimental reference in comparison with the typical values. This discrepancy is especially pronounced for Cu, for which there appears to be a few 100 keV difference. Unfortunately, we do not have an experimental value for that transition to verify the accuracy of our calculations directly. By considering the transitions $3d \rightarrow 2p$ and $2p \rightarrow 1s$ sequentially, we can estimate based on both our calculations and the experimental data, that the corresponding K_β transition should have an energy in the range 1800-1850 keV, which is quite far from the so-called typical value of 2126 keV. The typical value seems to correspond to the muon transitioning from a near-continuum state to the 1s orbital.

Our calculations indicate a splitting in energies due to the finite size of the nucleus. For example, when looking at the $4p \rightarrow 2s$ and $4d \rightarrow 2p$ transitions in Cu, a 35 keV difference can be noticed. This is caused by the involvement of 2s orbital in the former case, where the muonic density
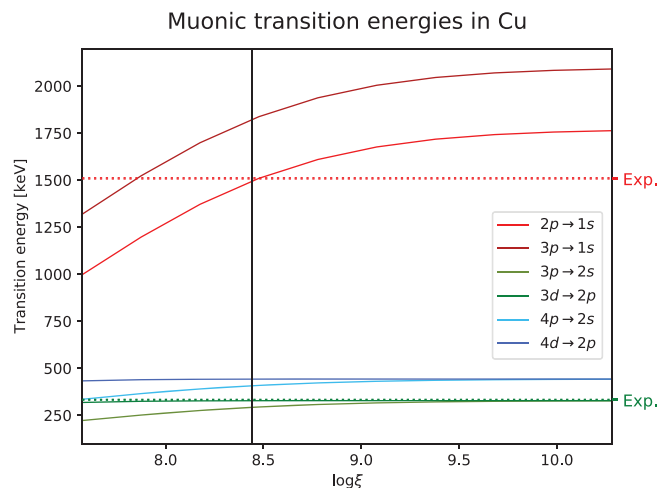
FIGURE 1 Dependence of muonic transition energies on the logarithm of the Gaussian nuclear charge distribution. We have calculated the curves for the transitions given in Table 1. The vertical line denotes the default value, $\xi = 2.767 \cdot 10^8$, for the Gaussian nuclear charge distribution. For comparison we have depicted the experimental transition energies with dashed horizontal lines.[33] The same experimental values are given in Table 1

at the nucleus is large and strongly affected by the nuclear size effects. To see how the width of the Gaussian nuclear charge distribution affects muonic transitions, we have calculated the transition energies in Cu for a range of ξ-values. The results can be seen in Figure 1. As the nuclear charge distribution is getting narrower, the transition energies are nearing the values with point-like nucleus in Table 1. In our calculations, it appears that the default Gaussian nuclear charge distribution parameters might not be optimal for precise prediction of muonic X-ray energies. From Figure 1, we can see that for the $2p \rightarrow 1s$ transition, the energies cover a wide range and the experimental value could be reproduced with another value for ξ. For the $3d \rightarrow 2p$ transition, however, the experimental value is above the plateau of point-like nucleus and modifying the nuclear charge distribution would not help. This kind of fitting of the Gaussian charge distribution should not be undertaken unless other corrections (eg, relativistic effects) are properly accounted for.

4.2 | Electronic structure effects

It is also interesting to ask how changes in the electronic wave function affect energy levels of the muon. We anticipated that higher muonic excitation levels become more affected by the presence of electrons compared to the lower ones where the muon lies closer to the nucleus. We investigated electronic effects on muonic X-ray energies by considering muons in differently charged ions, Ar^+ and Ar^-, and in different molecules, H_2O^- and CH_2O^- where the muon was centered on the nucleus of the oxygen atom. The results from CASSCF calculations are presented in Figure 2.

As expected, higher-level muonic transition energies vary more greatly between systems with different electronic structure. Notably the differences are larger for $p \rightarrow s$ transitions compared to $d \rightarrow p$ transitions. In both cases, the energy differences are positive, that is the muonic X-ray energies are larger for Ar^- compared to Ar^+ and similarly for H_2O^- compared with CH_2O^- This can be explained by considering that in the case of Ar, the larger number of electrons in Ar^- shifts upper muonic energy levels higher compared to Ar^+. Intuitively, similar reasoning should apply
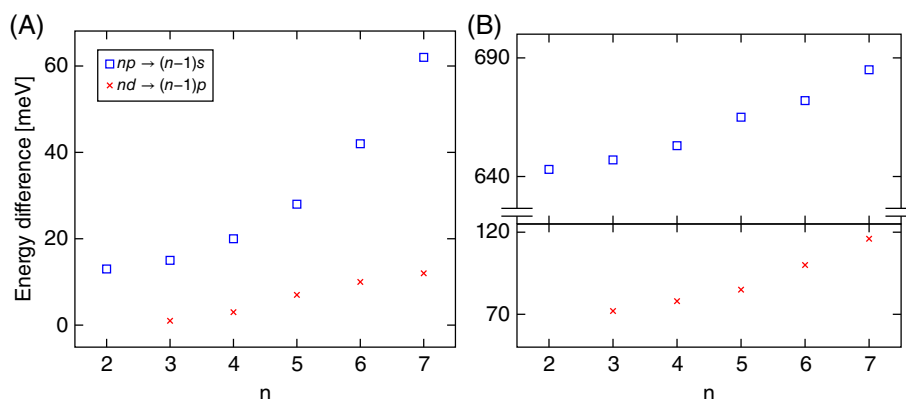
FIGURE 2 Energy differences between muonic transitions. Difference is calculated by **A)** subtracting the transition energy for Ar^+ from the corresponding one in Ar^-, **B)** subtracting the transition energy for CH_2O^- from the corresponding one in H_2O^-

to formaldehyde and water, where the electron density at oxygen in formaldehyde is lower due to different chemical environment and hybridization of the oxygen atom (sp^3 in water vs. sp^2 in formaldehyde). The trends seen in the graphs in Figure 2 show that transitions from higher-energy muonic states are expected to be more influenced by electronic structure. Finally, it should be mentioned that the muonic energy levels considered are still fairly low. In the case of hydrogen-like atoms, electronic 1s orbitals and muonic n_μs orbitals become of similar size when the muonic principal quantum number n_μ is 14. When the muon resides in the higher energy states, the shielding of nuclear charge by it is no longer as efficient.[29] In that case, electronic basis sets meant for the element with nuclear charge $Z - 1$ may not be accurate enough and the question of which basis sets to choose is no longer trivial. This should be kept in mind when one is interested in looking at states with higher muonic quantum number.

5 | CONCLUSIONS

In this work, we have developed primitive muonic basis sets for the elements in the first three rows and Cu. The use of the basis sets was demonstrated in many-electron-and-one-muon calculations of atoms and molecules to predict muonic X-ray energies. We re-emphasized the importance of considering a finite-sized nuclear model in calculations of muonic systems. Additionally, we studied the effects of chemical environment on muonic energy levels. Our results suggest two directions for future investigation. First, while using a Gaussian model for the nucleus can improve the accuracy of predicted muonic X-ray energies, the choice of default parameters might not be best for this application. We propose that comparing experimental muonic X-ray energies with corresponding predicted X-ray energies could be used to assess the nuclear charge distribution models and perhaps develop more accurate ones. This would first require considering the importance of several additional corrections such as vacuum polarization, spin-orbit coupling, and relativistic effects. Second, we demonstrated how changes in electronic structure influence muonic X-ray energies. In our calculations, the changes were less than 1 eV. However, by considering higher-energy muonic states, these effects are expected to become larger and hopefully more significant for spectroscopic applications. Studying it further would require development of new, larger, and possibly contracted muonic basis sets. We hope that by including the muonic basis sets in the OpenMolcas software, this work could aid in interpreting muonic X-ray spectra.

ORCID

Mihkel Ugandi [iD] http://orcid.org/0000-0002-8218-6966

REFERENCES

[1] M. Goli, S. Shahbazian, *Chemistry* **2016**, *22*(7), 2525.
[2] J. S. Möller, P. Bonfa, D. Ceresoli, F. Bernardini, S. J. Blundell, T. Lancaster, R. De Renzi, N. Marzani, I. Watanabe, S. Sulaiman, M. I. Mohamed-Ibrahim, *Phys. Scripta* **2013**, *88*(6), 068510.
[3] S. Blundell, *Contemp. Phys.* **1999**, *40*(3), 175.
[4] T. Yoshikawa, T. Honda, T. Takayanagi, *Chem. Phys.* **2014**, *440*, 135.
[5] K. Yamada, Y. Kawashima, M. Tachikawa, *J. Chem. Theory Comput.* **2014**, *10*(5), 2005.
[6] Y. Oba, T. Kawatsu, M. Tachikawa, *J. Chem. Phys.* **2016**, *145*(6), 064301.
[7] M. K. Kubo, *J. Phys. Soc. Jpn.* **2016**, *85*(9), 091015.
[8] K. Nagamine, *Introductory Muon Science*, Cambridge University Press, Cambridge. **2003**.
[9] B. Goulard, H. Primakoff, *Phys. Rev. C* **1974**, *10*(5), 2034.
[10] T. Suzuki, D. F. Measday, J. Roalsvig, *Phys. Rev. C* **1987**, *35*(6), 2212.
[11] N. Kazuhiko, T. Nagamoto, K. Kenya, T.U. Ito, W. Higemoto, M. Kita, A. Shinohara, P. Strasser, N. Kawamura, K. Shimomura, Y. Miyake, T. Saito, *Bull. Chem. Soc. Jpn.* **2012**, *85*(2), 228.
[12] K. Terada, K. Ninomiya, T. Osawa, S. Tachibana, Y. Miyake, M. Kubo, et al., *Sci. Rep.* **2014**, *4*, 5072.
[13] K. Ninomiya, M. K. Kubo, T. Nagatomo, W. Higemoto, T. U. Ito, N. Kawamura, P. Strasser, K. Shimomura, Y. Miyake, T. Suzuki, Y. Kobayashi, S. Sakamoto, A. Shinohara, T. Saito, *Anal. Chem.* **2015**, *87*(9), 4597.
[14] F. Moncada, D. Cruz, A. Reyes, *Chem. Phys. Lett.* **2012**, *539*, 209.
[15] F. Moncada, D. Cruz, A. Reyes, *Chem. Phys. Lett.* **2013**, *570*, 16.
[16] E. Posada, F. Moncada, A. Reyes, *J. Phys. Chem. A* **2014**, *118*(40), 9491.
[17] B. O. Roos, P. R. Taylor, P. E. Si, et al., *Chem. Phys.* **1980**, *48*(2), 157.
[18] C. P. Gonçalves, J. R. Mohallem, *Theor. Chem. Acc.* **2003**, *110*(6), 367.
[19] J. R. Mohallem, L. G. Diniz, A. S. Dutra, *Chem. Phys. Lett.* **2011**, *501*(4–6), 575.
[20] L. Visscher, K. G. Dyall, *At. Data Nucl. Data Tables* **1997**, *67*(2), 207.
[21] M. Klobukowski, *Chem. Phys. Lett.* **1993**, *214*(2), 166.
[22] J. A. Nelder, R. Mead, *Comput. J.* **1965**, *7*(4), 308.
[23] E. Jones, T. Oliphant, P. Peterson, et al., SciPy: Open source scientific tools for Python. 2001, http://www.scipy.org/ (accessed: August 18, 2018).
[24] P. O. Widmark, P. Å. Malmqvist, B. O. Roos, *Theor. Chem. Acc.* **1990**, *77*(5), 291.
[25] P. O. Widmark, B. J. Persson, B. O. Roos, *Theor. Chim. Acta* **1991**, *79*(6), 419.
[26] K. Pierloot, B. Dumez, P. O. Widmark, B. O. Roos, *Theor. Chem. Acc.* **1995**, *90*(2), 87.
[27] F. Aquilante, J. Autschbach, R. K. Carlson, L. F. Chibotaru, M. G. Delcey, L. De Vico, I. F. Galvan, N. Ferre, L. M. Frutos, L. Gagliardi, M. Garavelli, A. Giussani, C. E. Hoyer, G. Li Manni, H. Lischka, D. Ma, P. A. Malmqvist, T. Mueller, A. Nenov, M. Olivucci, T.B. Pedersen, D. Peng, F. Plasser,

B. Pritchard, M. Reiher, I. Rivalta, I. Schapiro, J. Segarra-Marti, M. Stenrup, D. G. Truhlar, L. Ungur, A. Valentini, S. Vancoillie, V. Veryazov, V. P. Vysotskiy, O. Weingart, F. Zapata, R. Lindh, *J. Comput. Chem.* **2016**, *37*(5), 506.

[28] OpenMolcas GitLab webpage, https://gitlab.com/Molcas/OpenMolcas (accessed: May 26, 2018)

[29] J. Mallow, J. Desclaux, A. Freeman, *Phys. Rev. A* **1978**, *17*(6), 1804.

[30] J. Mallow, J. Desclaux, A. Freeman, M. Weinert, *Hyperfine Interact.* **1981**, *8*(4), 455.

[31] C. Piller, C. Gugler, R. Jacot-Guillarmod, L. A. Schaller, L. Schellenberg, H. Schneuwly, G. Fricke, T. Hennemann, J. Herberz, *Phys. Rev. C* **1990**, *42*(1), 182.

[32] L. Schaller, *Muonic Atoms Spectroscopy*, The Future of Muon Physics Springer, **1992**, p. 48. Fribourg, Switzerland.

[33] R. Engfer, H. Schneuwly, J. Vuilleumier, H. Walter, A. Zehnder, *At. Data Nucl. Data Tables* **1974**, *14*(5–6), 509.

[34] M. Kubo, H. Moriyama, Y. Tsuruoka, S. Sakamoto, E. Koseto, T. Saito, K. Nishiyama, *J. Radioanal. Nucl. Chem.* **2008**, *278*(3), 777.

[35] R. Jenkins, R. Manne, R. Robin, C. Senemaud, *Pure Appl. Chem.* **1991**, *63*(5), 735.

SUPPORTING INFORMATION

Additional supporting information may be found online in the Supporting Information section at the end of the article.